

Schrödinger-Heisenberg Variational Quantum Algorithms

Zhong-Xia Shang^{1,2,3}, Ming-Cheng Chen^{1,2,3}, Xiao Yuan^{4,5}, Chao-Yang Lu^{1,2,3}, Jian-Wei Pan^{1,2,3}

¹Hefei National Laboratory for Physical Sciences at Microscale and Department of Modern Physics, University of Science and Technology of China, Hefei, Anhui 230026, China

²Shanghai Branch, CAS Centre for Excellence and Synergetic Innovation Centre in Quantum Information and Quantum Physics, University of Science and Technology of China, Shanghai 201315, China

³Shanghai Research Center for Quantum Sciences, Shanghai 201315, China

⁴Center on Frontiers of Computing Studies, Peking University, Beijing 100871, China

⁵School of Computer Science, Peking University, Beijing 100871, China

One sentence summary:

We propose a framework of virtual Heisenberg-circuit-enhanced variational quantum algorithms, which can noiselessly and effectively increase the circuit depth and hence the expressivity of quantum states, allowing more accurate realizations of variational quantum algorithms.

Abstract

Recent breakthroughs have opened the possibility to intermediate-scale quantum computing with tens to hundreds of qubits, and shown the potential for solving classical challenging problems, such as in chemistry and condensed matter physics. However, the high accuracy needed to surpass classical computers poses a critical demand to the circuit depth, which is severely limited by the non-negligible gate infidelity, currently around 0.1-1%. Here, by incorporating a virtual Heisenberg circuit, which acts effectively on the measurement observables, to a real shallow Schrödinger circuit, which is implemented realistically on the quantum hardware, we propose a paradigm of Schrödinger-Heisenberg variational quantum algorithms to resolve this problem. We choose a Clifford virtual circuit, whose effect on the Hamiltonian can be efficiently and classically implemented according to the Gottesman-Knill theorem. Yet, it greatly enlarges the state expressivity, realizing

much larger unitary t -designs. Our method enables accurate quantum simulation and computation that otherwise are only achievable with much deeper circuits or more accurate operations conventionally. This has been verified in our numerical experiments for a better approximation of random states and higher-fidelity solutions to the XXZ model and the electronic structure Hamiltonians of small molecules. Thus, together with effective quantum error mitigation, our work paves the way for realizing accurate quantum computing algorithms with near-term quantum devices.

Main text

Almost four decades after Richard Feynman put forward the idea of quantum computing¹, the quantum computational speedup has been experimentally confirmed recently in solid-state²⁻⁴ and photonic systems^{5,6}. However, those quantum computational advantage works focused on well-defined quantum sampling problems which were not designed practically useful. Therefore, the next important near-term milestone is to find algorithms for noisy intermediate-scale quantum (NISQ)⁷ devices to solve non-trivial practical problems that are intractable for classical computation.

One of the most promising NISQ applications is hybrid quantum-classical algorithms such as the variational quantum eigensolver (VQE)^{8,9} and variational quantum simulation (VQS) algorithms¹⁰⁻¹¹, which exploit different variational principles to compute the eigenstate energy and to simulate the dynamics of a Hamiltonian, respectively, tasks that are widely considered in combinatorial optimization problems¹², condensed matter physics¹³, and quantum chemistry¹⁴. A practical advantage of hybrid algorithms is their certain degrees of resilience to noise in the optimization and quantum hardware^{11,14-16}.

Hybrid algorithms generally use a shallow local unitary circuit (LUC) to approximate the target quantum state. Those states however could become trivial, obeying the entanglement area law¹⁷, with a very limited circuit depth (when considering its realistic implementation on NISQ devices). Indeed, the Lieb-Robinson bound¹⁸ indicates that the entanglement light cone restricts the propagation of correlations and, therefore, too shallow LUC cannot generate long-range entanglement. It has also been shown¹⁹ that classical algorithms can

efficiently evaluate expectation values of tensor product operators of the output states of shallow circuits with a constant depth.

However, the target quantum state, such as the ground state, could be highly non-trivial for a number of important Hamiltonians, such as interacting spins at critical points^{20,21}, topological quantum orders²²⁻²⁴, and interacting fermions in complex molecules²⁵. Solving or simulating these Hamiltonians by VQE or VQS algorithms usually require a relatively deep LUC with a depth that scales with the qubit number^{26,27}, making the implementation challenging with NISQ devices. Indeed, without an effective quantum error correction, the final fidelity of the quantum circuits drops exponentially with the number of gates. For example, a state-of-the-art random quantum circuit with 60 qubits and 24 depths³ ended up with a cross-entropy benchmarking fidelity as low as 0.037%. We thus need to significantly improve the NISQ hardware to implement those hybrid algorithms to a desired accuracy.

This situation can be summarized as a tradeoff between the fidelity of the LUC and its expressivity¹⁰ (i.e., the ability for the quantum circuits to “express” a sufficiently large volume of quantum states to include the target solution). To circumvent this problem, we propose a new framework of hybrid quantum-classical algorithms, enhanced by virtual Heisenberg circuits, which can noiselessly increase the effective circuit depth and thus simultaneously improve its expressivity and fidelity. Our algorithm belongs to the category of the hybrid ansatz²⁸⁻³². We call our scheme Schrödinger-Heisenberg (SH) variational quantum algorithms (VQA), which illustrates that the main idea is that, in addition to the physical unitary circuit, U , acting on the quantum states in the Schrödinger picture, we bring in a virtual circuit, T , acting on the target Hamiltonian H in the Heisenberg picture (see Fig. 1a). In the following, we consider SH-VQE as an example, but we note that the algorithm works for general VQAs. In this case, the energy expectation value $E(T, U) = \langle 0^{\otimes n} | U^\dagger T^\dagger H T U | 0^{\otimes n} \rangle$ of the system becomes

$$E(T, U) = \langle 0^{\otimes n} | U^\dagger H_T U | 0^{\otimes n} \rangle, \quad (1)$$

where the classically calculated transformed Hamiltonian $H_T = T^\dagger H T$ has the same energy spectrum as H . By properly choosing a relatively deep but noiseless T , the state $TU|0^{\otimes n}\rangle$ could explore the Hilbert space far outside the range of $U|0^{\otimes n}\rangle$ (see Fig. 1b) and hence can obtain a lower and more accurate ground-state energy than conventional VQE.

We show a workflow of SH-VQE together with a comparison to conventional VQE in Figure 1c. In analog to VQE, both the real Schrödinger circuit U and the virtual Heisenberg circuit T in SH-VQE are parametrized and updated when minimizing the expectation value $E(T, U)$. The key feature of SH-VQE is that only a shallow LUC U is physically implemented, whereas the relatively deep circuit T is performed virtually and noiselessly using a classical computer.

We first show how to effectively measure H_T . In general, the target Hamiltonian H could be expressed as a linear sum of multi-qubit Pauli terms $H = \sum_{i=1}^m g_i P_i$, where $P_i \in \{\sigma_I, \sigma_X, \sigma_Y, \sigma_Z\}^{\otimes n}$. Then we can measure each P_i with a total number of samples $(\frac{m}{\epsilon^2}) \sum_i g_i^2 \text{Var}[P_i]$, proportional to the number of terms (m) in the Hamiltonian⁹, to evaluate the energy expectation value within an error of ϵ . Here $\text{Var}[P_i] = \langle P_i^2 \rangle - \langle P_i \rangle^2$. We can similarly measure H_T , by similarly decomposing each $T^\dagger P_i T$ into Pauli strings. While most practical Hamiltonians H only contain a polynomial number of terms, this might not be the case for $T^\dagger P_i T$ or H_T , after the transformation (See SI).

Here we propose a structure of the Heisenberg circuit that also leads to efficiently measurable $T^\dagger P_i T$ or H_T . The circuit consists of two parts (Fig. 1a), where the first part is an arbitrary Clifford circuit that can be decomposed into a sequence of $O(n^2)$ basic gates from the set $\{H, S, \text{CNOT}\}$, and the second part is a layer of single qubit gates. The first part realizes discrete gates such as CNOT to build correlations between any two qubits and the second part makes them continuous. The Clifford circuit maps the multi-qubit Pauli group to itself, which conserves the number of terms of the Hamiltonian. Also, the Gottesman-Knill theorem³³ indicates that calculating the transformed Hamiltonian is easy. While the second part might increase the number of terms of the Hamiltonian, the overhead becomes finite for Hamiltonians H consisting of only k -weight terms, i.e., the Pauli operators $\{\sigma_X, \sigma_Y, \sigma_Z\}$ act on at most k qubits. After a layer of single qubit gates acted on the Hamiltonian, the number of terms m' keeps polynomial and bounded by $m' \leq \min[m, C_n^k](4^k - 1)$, where C_n^k is the total number of possible k -weight terms in n -qubit Pauli group. We note that one can change this part into other easier or more complex circuits for different Hamiltonians, considering the trade-off between the circuit power and the measurement cost.

We begin to study the expressivity of the circuit in SH-VQE. We consider the expressivity measure using the method of quantum complex projective t -design (t -design)³⁴, which requires that the distribution of the output states has equal moments up to the t^{th} order to a Haar uniform distributed states from the whole Hilbert space. Intuitively, as illustrated in Fig. 2a, a higher t -design indicates a more uniform and denser state distribution in the Hilbert space, and vice versa. In general, a LUC of depth $O(nt^{10})$ is needed to generate a t -design³⁵, and the Clifford circuits can produce a 3-design^{36,37}. Using the tight Page's theorem³⁸, we define the logarithmic difference of entanglement entropy 错误!未找到引用源。 as

$$\Delta_t = \log(E_{\text{Haar}}[\text{Tr}(\rho_{n/2}^t)]) - \log(E_{\text{SH}}[\text{Tr}(\rho_{n/2}^t)]) \quad (2)$$

to identify the order of expressivity of SH-VQE, where $\rho_{n/2}$ is the reduced half system density matrix, E_{Haar} is the average over Haar random states, and E_{SH} is the average over the quantum states $TU|0^{\otimes n}\rangle$. If Δ_t increases and approaches 0, it means that $TU|0^{\otimes n}\rangle$ is a t -design.

Figure 2b shows a comparison of the expressivity of SH-VQE versus VQE through a numerical experiment on a 12-qubit system. In the VQE setting, we run a random LUC and, at different depths, and calculate Δ_t to characterize the t -design. In the SH-VQE setting, we implement both the real Schrödinger circuits U and the virtual Heisenberg circuits T which are pure Clifford consisting of 500 random gates from {H, S, CNOT}. The key observation for both cases is the critical depths when the Δ_t measure increases to and saturates at around 0. It is evident that the Δ_t curves for SH-VQE rise much more rapidly than that for VQE for all t values from 3 to 12. The rising curve for SH-VQE quickly hits the saturation point at a Schrödinger circuit depth of ~ 2 , while the VQE curve arrives at a much deep depth of ~ 36 . This indicates that SH-VQE can indeed effectively reduce the gate depth by more than one order of magnitude to achieve the same level of expressivity. For a higher number of qubits, we expect an even more dramatic advantage, which can be inferred from a qubit-size dependent test of depth reduction as shown in Fig. S3. Therefore, we expect our approach to be critical for enhancing the expressivity of intermediate-scale quantum devices.

The above results indicate that we can use current NISQ hardware to effectively run deep quantum circuits while maintaining high fidelity. Particularly, based on a two-qubit gate fidelity of 99.5%, the SH-VQE can allow us to run, for instance, a 12-qubit 4-depth quantum circuit with an output fidelity of 90%, which would otherwise demand a two-qubit gate fidelity of 99.95% (currently unrealistic) and 40 depths in conventional VQE (Fig. S2). Note that shallow LUC or Clifford circuits alone can only generate small design orders, but a combination of them can achieve high expressivity.

We consider an example of the XXZ spin model with a periodic boundary condition

$$H_{XXZ} = \sum_{i=1}^n [\sigma_i^x \sigma_{i+1}^x + \sigma_i^y \sigma_{i+1}^y + \Delta \sigma_i^z \sigma_{i+1}^z] \quad (3)$$

to demonstrate a kind of working flow of SH-VQE. At the critical point $\Delta = 1$, the XXZ model is equivalent to the Heisenberg model whose ground state has a logarithmic scaling of entanglement entropy^{20,21}, and hence cannot be prepared by a constant-depth LUC. Here we use SH-VQE with a shallow (Schrödinger) LUC and a virtual (Heisenberg) circuit to solve the problem. Since we aim to boost the performance of the NISQ experiments, we use the hardware efficient ansatz¹⁴ for the real Schrödinger circuit even though this may lead to barren plateau problems³⁹, where each circuit layer composes a layer of controlled-Z (CZ) entangling gates and a layer of parametrized arbitrary single-qubit gates (denoted as $\vec{\theta}$).

For the Heisenberg circuit, the single-qubit gate layer is parametrized with parameters $\vec{\phi}$. And we restrict the Clifford part to graph circuits⁴⁰ where only commuting CZ gates are used. We separate the graph circuit to patterns of different connectivity with translational invariant symmetry. More concretely, for an n -qubit circuit, we can set $\lfloor n/2 \rfloor$ elementary graphs (For the j^{th} elementary graph, each node i is connected with node $i+j$. $\lfloor \cdot \rfloor$ is the floor function.). As each elementary graph can be turned on or turned off, the total number of possible patterns is $2^{\lfloor n/2 \rfloor}$ and we use a $\lfloor n/2 \rfloor$ -bit string to label all the possible patterns such as ‘01001...’, where 0 means the corresponding elementary graph is turned on whereas 1 means off (Fig. 3a). To efficiently search through a exponentially large space of Clifford gate patterns, we borrow the idea from differentiable quantum architecture search⁴¹, where each elementary TI graph is turned on independently according to a probability described by a two-parameter softmax function⁴². Thus, only $\lfloor n/2 \rfloor \times 2$

parameters (denoted as $\vec{\alpha}$) are needed to implement the discrete search of the huge Clifford patterns. Therefore, the circuit ansatz for the SH-VQE is

$$T(\vec{\alpha}, \vec{\phi})U(\vec{\theta})|0^{\otimes n}\rangle, \quad (4)$$

where $\vec{\alpha}$ and $\vec{\phi}$ represents all configurations of the virtual (Heisenberg) circuit T and $\vec{\theta}$ are the continuous parameters in the single-qubit gates inside the real (Schrödinger) circuit U . The parameters $\vec{\alpha}$ are used to generate samples of different circuits and the cost function is the average of the Hamiltonian expectation values of these circuits under the same gate parameters $\vec{\theta}$ and $\vec{\phi}$. The SH-VQE method then optimizes over all the parameters to search for the ground state of the Hamiltonian.

In our numerical simulation, we consider an 8-spin XXZ model with a depth-4 circuit U and 4 elementary TI graphs of the Clifford layer as shown in Fig. 3a. We show the energy expectation and the evolution of the possibilities of all 16 configurations during the optimization as functions of the number of iterations in Fig. 3b. When the energy expectation is converged, the probabilities of the candidate circuit structures concentrate to the optimal configuration, the fully connected graph ‘1111’. In Fig. 3c, we show the optimal energies of all the 16 candidate circuit configurations, which verifies that the optimal configuration is indeed the fully connected graph ‘1111’.

We further solve larger models up to 16 spins to show the improvement of SH-VQE compared with conventional VQE using the same Schrödinger circuits. For SH-VQE, we directly use the generalized fully connected graph circuits as the Clifford part. In Fig. 4a, we show the distance between the optimized energy and the exact ground-state energy as a function of the Schrödinger circuit depth, from which we see that the SH-VQE can obtain lower energy than the VQE under the same depth. The advantage of the SH-VQE is also evident from the ground-state fidelities in Fig. 4b. Under the same circuit depth, the SH-VQE obtains higher fidelities than the VQE. A direct comparison of their fidelities is summarized in the left panel of Fig. 4b, with an average of 25.2% fidelity improvement.

To further demonstrate the practical value of our algorithm, we implement our algorithm to solve the electronic structure problems of H_4 and H_2O molecules following the same workflow as the above. The H_4 molecule corresponds to an 8-qubit Hamiltonian. For the

H₂O molecule, we use the active space method⁴³ to create an effective 10-qubit Hamiltonian (ignoring the 1s and 2a1 orbitals of O and considering 6 active electrons). Since the SH-VQA has the Pauli weight restriction, we use the Bravyi-Kitaev mapping which transforms an M -mode fermionic Hamiltonian to a spin Hamiltonian of $O(\log_2 M)$ Pauli weight⁴⁴⁻⁴⁵. The results are shown in Fig. 5, where we can see SH-VQE can reach the chemical accuracy with much shallower Schrödinger circuit depth than VQE.

We emphasize that the states $TU|0^{\otimes n}\rangle$ is both hard to prepare on NISQ devices, as it requires to implement the relatively deep T circuit, and hard to simulate on classical computers, as it can be treated as Clifford circuits with non-stabilizer input states. However, within the SH-VQE framework, the operator expectation values under these states can be efficiently evaluated for shallow LUC¹⁹. Therefore, our work also indicates a computational complexity separation between the simulation of quantum circuit and the estimation of their quantum expectations.

We also want to give a discussion on the trainability of SH-VQA. A known result is that in general, an ansatz with high expressibility may lead to low trainability⁴⁶. However, this doesn't mean the trainability of SH-VQA is poor. The t -design results shown in Fig. 2 should be understood as the enlargement of the exploring range of NISQ devices but not the actual expressibility of the ansatz for specific problems. Like VQE, we can also create the problem-inspired ansatz of high trainability such as the Unitary Coupled Cluster⁹ and the Hamiltonian Variational Ansatz¹³ within the SH-VQA framework. Naively, since the Heisenberg circuit serves as a basis transformation, we can consider the quantum hardware capability to think of or optimize a suitable Heisenberg part to make those problem-inspired hardware-inefficient ansatzes easier to implement on NISQ devices. We summarize the discussions of the expressibility and the trainability of SH-VQA in Fig. S5.

In summary, we have introduced a novel variational quantum algorithm, the SH-VQA, to efficiently extend the circuit depth of near-term noisy quantum processors. By virtually introducing a relatively deep and non-local Clifford circuits, we show that the expressivity of shallow quantum circuits can be significantly enhanced, without sacrificing the fidelity. We use the XXZ model to demonstrate the workflow of SH-VQA and further demonstrate the practical values of SH-VQA by solving small molecules. Our method is directly

applicable to current quantum hardware and is compatible with most existing quantum algorithms. Leveraging quantum error mitigation^{11,14,15}, our work pushes near-term quantum hardware into wide non-trivial applications for solving static and dynamic quantum problems, quantum optimization, quantum machine learning, etc¹⁰.

We use the Qulacs⁴⁷ and the Qiskit⁴⁸ packages for parts of simulations.

References and notes

1. Feynman, Richard P. "Simulating physics with computers." *Feynman and computation*. CRC Press, 2018. 133-153.
2. Arute, Frank, et al. "Quantum supremacy using a programmable superconducting processor." *Nature* 574.7779 (2019): 505-510.
3. Zhu, Qingling, et al. "Quantum computational advantage via 60-qubit 24-cycle random circuit sampling." *Science Bulletin* 67.3 (2022): 240-245.
4. Wu, Yulin, et al. "Strong quantum computational advantage using a superconducting quantum processor." *Physical review letters* 127.18 (2021): 180501.
5. Zhong, Han-Sen, et al. "Quantum computational advantage using photons." *Science* 370.6523 (2020): 1460-1463.
6. Zhong, Han-Sen, et al. "Phase-programmable Gaussian boson sampling using stimulated squeezed light." *Physical review letters* 127.18 (2021): 180502.
7. Preskill, John. "Quantum computing in the NISQ era and beyond." *Quantum* 2 (2018): 79.
8. Peruzzo, Alberto, et al. "A variational eigenvalue solver on a photonic quantum processor." *Nature communications* 5.1 (2014): 1-7.
9. McClean, Jarrod R., et al. "The theory of variational hybrid quantum-classical algorithms." *New Journal of Physics* 18.2 (2016): 023023.
10. Cerezo, Marco, et al. "Variational quantum algorithms." *Nature Reviews Physics* 3.9 (2021): 625-644.

11. Endo, Suguru, et al. "Hybrid quantum-classical algorithms and quantum error mitigation." *Journal of the Physical Society of Japan* 90.3 (2021): 032001.
12. Farhi, Edward, Jeffrey Goldstone, and Sam Gutmann. "A quantum approximate optimization algorithm." *arXiv preprint arXiv:1411.4028* (2014).
13. Wecker, Dave, Matthew B. Hastings, and Matthias Troyer. "Progress towards practical quantum variational algorithms." *Physical Review A* 92.4 (2015): 042303.
14. Kandala, Abhinav, et al. "Hardware-efficient variational quantum eigensolver for small molecules and quantum magnets." *Nature* 549.7671 (2017): 242-246.
15. Temme, Kristan, Sergey Bravyi, and Jay M. Gambetta. "Error mitigation for short-depth quantum circuits." *Physical review letters* 119.18 (2017): 180509.
16. Li, Ying, and Simon C. Benjamin. "Efficient variational quantum simulator incorporating active error minimization." *Physical Review X* 7.2 (2017): 021050.
17. Brandao, Fernando GSL, and Michał Horodecki. "Exponential decay of correlations implies area law." *Communications in mathematical physics* 333.2 (2015): 761-798.
18. Bravyi, Sergey, Matthew B. Hastings, and Frank Verstraete. "Lieb-Robinson bounds and the generation of correlations and topological quantum order." *Physical review letters* 97.5 (2006): 050401.
19. Bravyi, Sergey, David Gosset, and Ramis Movassagh. "Classical algorithms for quantum mean values." *Nature Physics* 17.3 (2021): 337-341.
20. Vidal, Guifre, et al. "Entanglement in quantum critical phenomena." *Physical review letters* 90.22 (2003): 227902.
21. Latorre, José Ignacio, Enrique Rico, and Guifré Vidal. "Ground state entanglement in quantum spin chains." *arXiv preprint quant-ph/0304098* (2003).
22. Kitaev, Alexei, and John Preskill. "Topological entanglement entropy." *Physical review letters* 96.11 (2006): 110404.
23. Levin, Michael, and Xiao-Gang Wen. "Detecting topological order in a ground

- state wave function." *Physical review letters* 96.11 (2006): 110405.
24. Chen, Xie, Zheng-Cheng Gu, and Xiao-Gang Wen. "Local unitary transformation, long-range quantum entanglement, wave function renormalization, and topological order." *Physical review b* 82.15 (2010): 155138.
 25. Bravyi, Sergey, et al. "Tapering off qubits to simulate fermionic Hamiltonians." *arXiv preprint arXiv:1701.08213* (2017).
 26. Huang, Yichen, and Xie Chen. "Quantum circuit complexity of one-dimensional topological phases." *Physical Review B* 91.19 (2015): 195143.
 27. Ho, Wen Wei, and Timothy H. Hsieh. "Efficient variational simulation of non-trivial quantum states." *SciPost Physics* 6.3 (2019): 029.
 28. Takeshita, Tyler, et al. "Increasing the representation accuracy of quantum simulations of chemistry without extra quantum resources." *Physical Review X* 10.1 (2020): 011004.
 29. Mizukami, Wataru, et al. "Orbital optimized unitary coupled cluster theory for quantum computer." *Physical Review Research* 2.3 (2020): 033421.
 30. Huggins, William J., et al. "A non-orthogonal variational quantum eigensolver." *New Journal of Physics* 22.7 (2020): 073009.
 31. Yuan, Xiao, et al. "Quantum simulation with hybrid tensor networks." *Physical Review Letters* 127.4 (2021): 040501.
 32. Zhang, Shi-Xin, et al. "Variational quantum-neural hybrid eigensolver." *Physical Review Letters* 128.12 (2022): 120502.
 33. Gottesman, Daniel. "The Heisenberg representation of quantum computers." *arXiv preprint quant-ph/9807006* (1998).
 34. Hoggar, Stuart G. "t-Designs in projective spaces." *European Journal of Combinatorics* 3.3 (1982): 233-254.
 35. Brandao, Fernando GSL, Aram W. Harrow, and Michał Horodecki. "Local random quantum circuits are approximate polynomial-designs." *Communications in Mathematical Physics* 346.2 (2016): 397-434.

36. Zhu, Huangjun. "Multiqubit Clifford groups are unitary 3-designs." *Physical Review A* 96.6 (2017): 062336.
37. Zhu, Huangjun, et al. "The Clifford group fails gracefully to be a unitary 4-design." *arXiv preprint arXiv:1609.08172* (2016).
38. Liu, Zi-Wen, et al. "Entanglement, quantum randomness, and complexity beyond scrambling." *Journal of High Energy Physics* 2018.7 (2018): 1-62.
39. McClean, Jarrod R., et al. "Barren plateaus in quantum neural network training landscapes." *Nature communications* 9.1 (2018): 1-6.
40. Hein, Marc, et al. "Entanglement in graph states and its applications." *arXiv preprint quant-ph/0602096* (2006).
41. Zhang, Shi-Xin, et al. "Differentiable quantum architecture search." *arXiv preprint arXiv:2010.08561* (2020).
42. The possibility of picking a graph $\vec{k} = 'k_1 k_2 \dots k_{\lfloor n/2 \rfloor}'$ is described by the product of $\lfloor n/2 \rfloor$ independent softmax functions $\prod_{i=1}^{\lfloor n/2 \rfloor} \frac{\exp(\alpha_{i,k_i})}{\exp(\alpha_{i,0}) + \exp(\alpha_{i,1})}$.
43. Rossmannek, Max, et al. "Quantum HF/DFT-embedding algorithms for electronic structure calculations: Scaling up to complex molecular systems." *The Journal of Chemical Physics* 154.11 (2021): 114105.
44. McArdle, Sam, et al. "Quantum computational chemistry." *Reviews of Modern Physics* 92.1 (2020): 015003.
45. Bravyi, Sergey B., and Alexei Yu Kitaev. "Fermionic quantum computation." *Annals of Physics* 298.1 (2002): 210-226.
46. Holmes, Zoë, et al. "Connecting ansatz expressibility to gradient magnitudes and barren plateaus." *PRX Quantum* 3.1 (2022): 010313.
47. Suzuki, Yasunari, et al. "Qulacs: a fast and versatile quantum circuit simulator for research purpose." *Quantum* 5 (2021): 559.
48. Cross, Andrew. "The IBM Q experience and QISKit open-source quantum computing software." *APS March meeting abstracts*. Vol. 2018. 2018.

49. The data is from <https://www.polyu.edu.hk/ama/staff/xjchen/sphdesigns.html>.
50. Arouri, Yazan, and Mohammad Sayyafzadeh. "An accelerated gradient algorithm for well control optimization." *Journal of Petroleum Science and Engineering* 190 (2020): 106872.

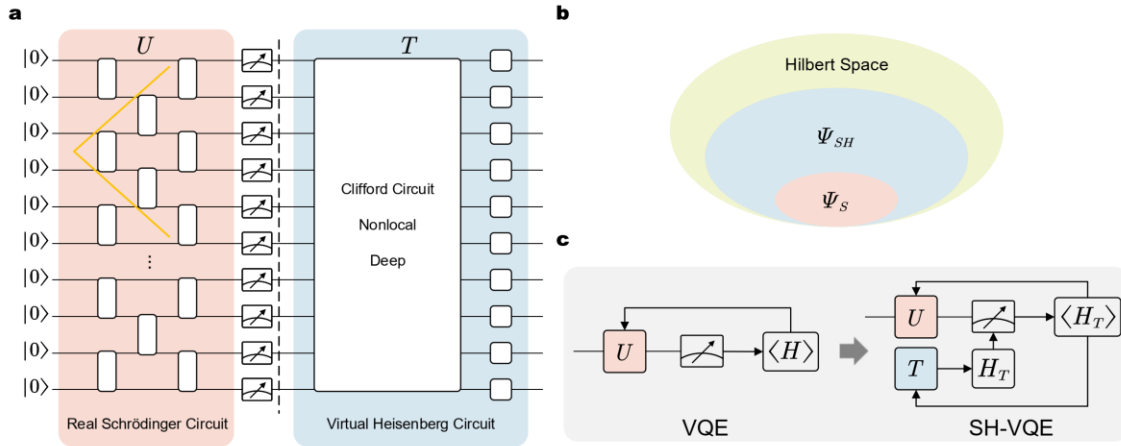


Fig. 1| SH-VQE. (a): The SH-VQE circuit. The circuit is composed of the Schrödinger circuit U and the Heisenberg circuit T , where U is the local unitary circuit running on real quantum computers and T is the virtual circuit acted on the Hamiltonian consisting of two parts --- the Clifford part and the single qubit layer. The architecture we use for U throughout this work is layers of parallel 2-qubit gates, which has a well-defined light cone that constrains the propagation of correlations and entanglements. **(b):** Improvements of SH-VQE. By adding the virtual circuit, $TU|0^{\otimes n}\rangle$ is able to explore more of the Hilbert space compared with $U|0^{\otimes n}\rangle$ in conventional VQE and the trainable Hilbert space is much larger than the conventional VQE. **(c):** Algorithm structure comparison between VQE and SH-VQE. The transformed Hamiltonian H_T replaces H in SH-VQE. We update parameters in both U and T to minimize the expectation value of H_T .

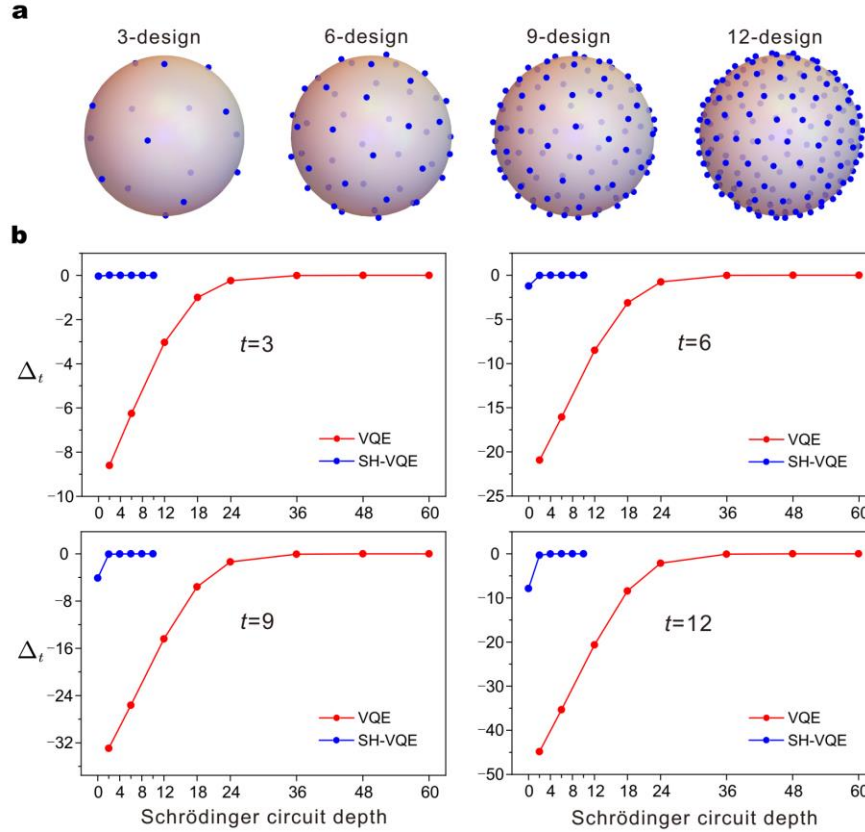


Fig. 2/SH-VQE expressivity. (a): Illustration of the relationship between expressivity and the t -design. We show the point distribution on the Bloch sphere of different design orders $t = 3, 6, 9, 12$. We can see that distributions of higher orders of t -design are more even and dense in the whole space⁴⁹. **(b):** Comparison of the expressivity measure Δ_t between VQE and SH-VQE for 12-qubits with $t = 3, 6, 9, 12$. The structure of the Clifford part is formed by 500 randomly picked basic Clifford gates in the set $\{H, S, CNOT\}$ (uniformly select a qubit then uniformly select a gate). The other parts including the two-qubit blocks in Schrödinger LUC and gates in the Heisenberg single qubit layer are random gates drawn from the Haar measure. The zero-depth setting in SH-VQE can be understood as the performance of the Clifford circuit. Since Clifford circuit can generate 3-design, Δ_t approaches 0 for $t = 3$ whereas below 0 in other cases. We observe that the expressivity of SH-VQE with Schrödinger circuit depth of 2 is already better than the VQE with depth of 20. Schrödinger circuit of depth greater than 6 combined with Heisenberg circuit is believed to generate the maximally scrambled states since values of Δ_t from $t = 3$ to $t = 12$ are all zero³⁸.

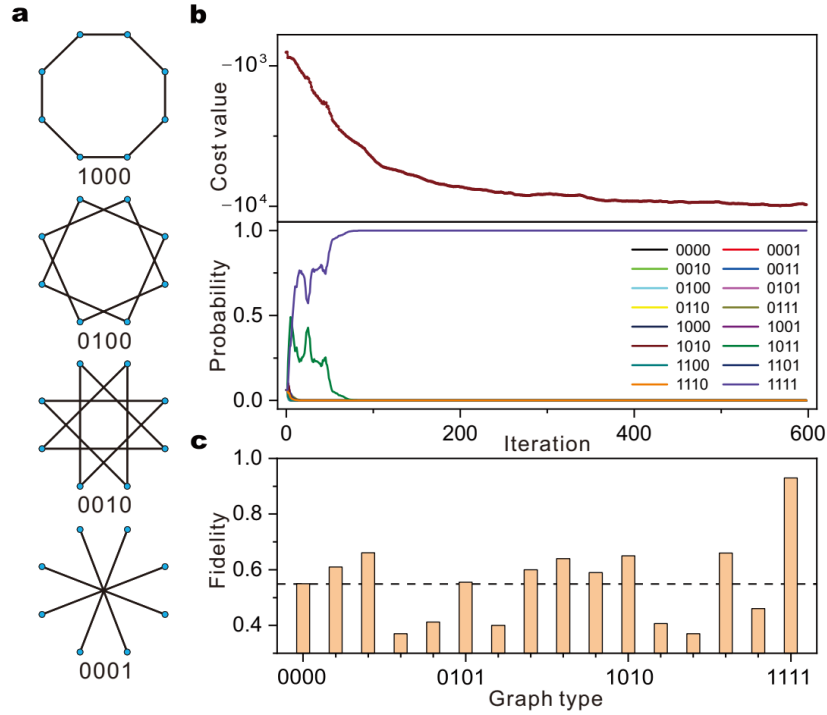


Fig. 3| Searching the Clifford circuit for XXZ model. (a): The 4 elementary graphs and their corresponding code strings for $n=8$ TI graphs. **(b): Upper Panel:** Minimizing the cost function to search for the best graph. Parameters contain both gate parameters and probability parameters. The cost function is the sum of the Hamiltonian expectation values of circuits sampled from $\vec{\alpha}$ under the same gate parameters. The number of samples at each iteration is 800. The initial gate parameters are chosen to be translationally invariant. **Lower Panel:** Probabilities of all 16 graphs as functions of iteration times. All graphs have the same probabilities at the beginning. The probability of the fully connected graph ‘1111’ becomes 1 as the iteration times grow. The optimization algorithm used for circuit structure searching is adam-SPSA⁵⁰. **(c):** Direct comparisons between different graphs. The dashed line is the result of the graph type: ‘0000’ i.e. without Heisenberg circuit. The fully connected graph shows great improvements and is indeed the best choice. There exist graphs which have worse performance than ‘0000’.

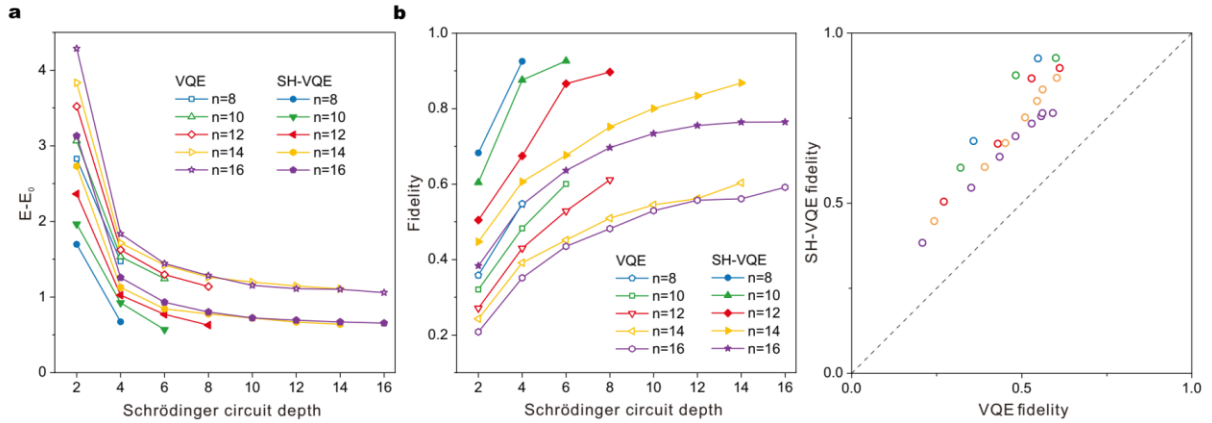


Fig. 4 | Comparisons of SH-VQE and VQE on solving the XXZ model. Using VQE and SH-VQE to solve 8, 10, 12, 14, 16-qubit XXZ model. Fully connected graphs are used as the Clifford layer. Great improvements can be observed by adding the Heisenberg circuit. **(a):** Comparison of energy. As the cost function, energy is the most intuitive value to show improvements of SH-VQE. The difference between the optimized energy and the exact ground energy as functions of RSC depth are plotted, from which we can see that SH-VQE can obtain lower energy than VQE using the same depth. VQE and SH-VQE of the same Schrödinger circuit depth share the same color. **(b):** Comparison of ground state fidelities. **Left Panel:** We calculated the fidelities between the converged states corresponding to points in (a) and the exact ground states of the XXZ Hamiltonians. Under the same LUC depth, SH-VQE can obtain much higher fidelities. Under the same fidelities, SH-VQE requires much lower Schrödinger circuit depth. **Right Panel:** Points with coordinates $(x, y) = (\text{VQE Fidelity}, \text{SH-VQE Fidelity})$ of every qubit number (different colors) and Schrödinger depth settings are plotted. All points in the up-left area show performance improvements of SH-VQE clearly (25.2% on average with 6.0% standard error). Each point is the best result obtained from 20 sets of random initial parameters.

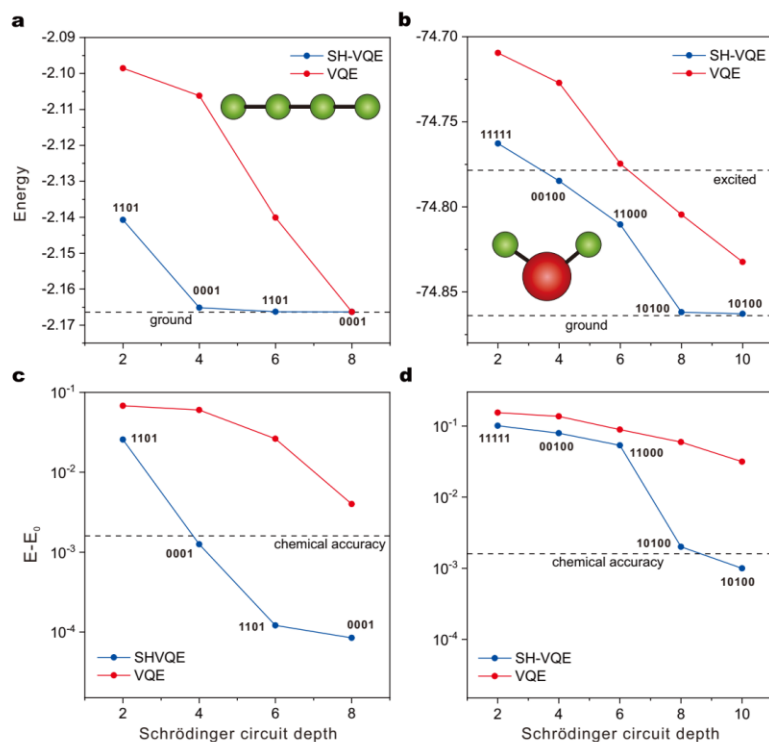


Fig. 4 | Comparisons of SH-VQE and VQE on solving small molecules. Using VQE and SH-VQE to solve the 8-qubit Hamiltonian of the H₄ molecule the bond distance 1.0 Angstrom and the 10-qubit Hamiltonian of the H₂O molecule of the bond distance 1.5 Angstrom. The binary strings around the SH-VQE data label the searched optimal graph circuits. **(a, b):** Solved energy as a function of Schrödinger circuit depth. **(c, d):** Absolute energy differences a function of Schrödinger circuit depth. From the results we can see SH-VQE can reach the chemical accuracy with much shallower Schrödinger circuit depth than VQE.

Supplementary Information for

Schrödinger-Heisenberg Variational Quantum Algorithms

¹Hefei National Laboratory for Physical Sciences at Microscale and Department of Modern Physics, University of Science and Technology of China, Hefei, Anhui 230026, China

²Shanghai Branch, CAS Centre for Excellence and Synergetic Innovation Centre in Quantum Information and Quantum Physics, University of Science and Technology of China, Shanghai 201315, China

³Shanghai Research Center for Quantum Sciences, Shanghai 201315, China

⁴Center on Frontiers of Computing Studies, Peking University, Beijing 100871, China

1. Measurement cost

For variational hybrid quantum-classical algorithms, a key step is to evaluate operators' expectation values. Typically, we use the so called operator averaging method, which has no requirements on circuits but requires a large number of measurements.

Without loss of generality, we consider a simple original Hamiltonian H , which is composed of only one Pauli operator. Consider P_h to be the Pauli operator we want to evaluate $\langle P_h \rangle = \text{tr}(\rho P_h)$, the variance of measuring P_h is $\text{Var}[P_h]_\rho = \text{tr}(\rho P_h^2) - \text{tr}(\rho P_h)^2$. If we repeat the measurement for N_1 times, the variance becomes

$$\text{Var}[P_h]_\rho \rightarrow \frac{\text{Var}[P_h]_\rho}{N_1} \quad (1.1)$$

If we want to reach an accuracy of ϵ , the number of measurements we need is

$$N_1 = \frac{\text{Var}[P_h]_\rho}{\epsilon^2} \quad (1.2)$$

Consider we act a circuit T to the Pauli operator P_h :

$$P_h \rightarrow T^\dagger P_h T = \sum_{i=1}^{m_h} c_i P_i \quad (1.3)$$

where $\sum_{i=1}^{m_h} c_i^2 = 1$. The circuit transforms P_h into m_h part. For the corresponding state $\rho_T = T^\dagger \rho T$, the variance is unchanged under the transformation $\text{Var}[P_h]_\rho = \text{Var}[T^\dagger P_h T]_{\rho_T}$. However, we need measure each term individually so the effective variance of those measurement does increase. One natural way is to repeat N_2/m_h

measurements to evaluate each one of Pauli terms and sum them. The variance under this way is

$$\sum_{i=1}^{m_h} \frac{m_h c_i^2 \text{Var}[P_i]_{\rho_T}}{N_2} \quad (1.4)$$

If we want to reach the same accuracy of ϵ , the number of measurements N_2 we need is

$$N_2 = \frac{m_h \sum_{i=1}^{m_h} c_i^2 \text{Var}[P_i]_{\rho_T}}{\epsilon^2} \approx m_h \frac{\text{Var}[P_h]_{\rho}}{\epsilon^2} = m_h N_1 \quad (1.5)$$

The approximation above is because every $\langle P_i \rangle$ can be treated as an expectation value of a Bernoulli random variable $\langle P_i \rangle = p_1 * 1 + p_{-1} * (-1)$ and the variance is bounded by $4p_1 p_{-1} \leq 1$. So, we assume the variances of Pauli terms are at the same level. From Eq. (1.5) we can see m_h must be controlled at a tolerable level, which explains why the structure of VHC must be restricted. This conclusion does not change even if one groups commuting terms.

Another point worth mentioning is that assigning N_2/m_h measurements to evaluate each one of Pauli terms is not the best choice. One can treat this as an optimization problem

$$\begin{aligned} \text{minimize: } & f(p_i) = \sum_i \frac{c_i^2 \text{Var}[P_i]_{\rho_T}}{N_2 p_i} \\ \text{subject to: } & \sum_i p_i = 1 \text{ and } p_i \geq 0, i = 1, \dots, m_h \end{aligned} \quad (1.6)$$

This problem can be easily solved using Lagrange multiplier method under the assumption that the variances of Pauli terms are at the same level and the best choice is $p_i = |c_i| / \sum_{i=1}^{m_h} |c_i|$ (which won't change the basic conclusion). Another choice is $p_i = c_i^2$. At first look, this choice should be better than the uniform choice $p_i = 1/m_h$ as the term with bigger variance is assigned with more measurements. However, they actually have the same performances

$$\sum_{i=1}^{m_h} \frac{c_i^2 \text{Var}[P_i]_{\rho_T}}{N_2 c_i^2} = \frac{\sum_{i=1}^{m_h} \text{Var}[P_i]_{\rho_T}}{N_2} \approx \sum_{i=1}^{m_h} \frac{m_h c_i^2 \text{Var}[P_i]_{\rho_T}}{N_2} \quad (1.7)$$

2. Circuit expressivity and hardware requirements

More detailed 12-qubit simulation results of expressivity comparisons between SH-VQE circuits and VQE circuits are shown in Fig.S1. From Fig.S1, we observe that by using the idea of SH-VQE, a quantum hardware of only 4-depth may have the close potential to a 40-depth hardware running VQE. This provides us a significant relief on the requirement of quantum gate fidelities in practical experiments. We show such reduction in Fig.S2.

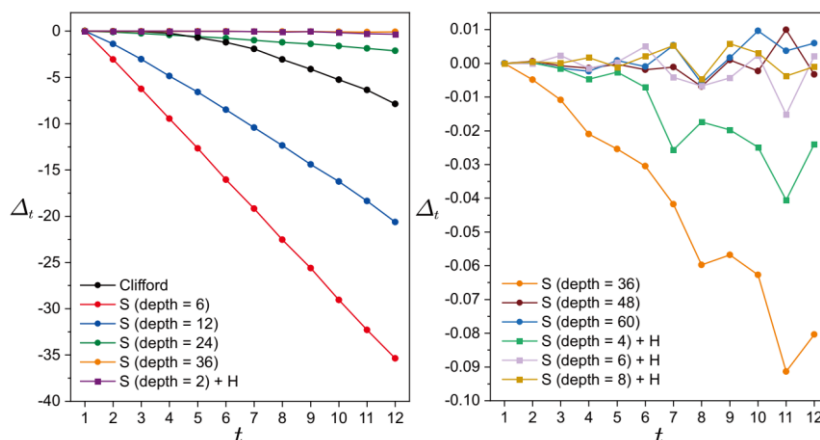


Figure S1: Values of 12-qubit Δ_t from $t=1$ to $t=12$ with different circuit settings. SH-VQE circuits of very shallow Schrödinger depth have the expressivity close to very deep VQE circuit. The Clifford circuits as reference can generate 3-design and good approximation of the 4-design. SH-VQE circuits of Schrödinger depth 6 is believed to generate max scrambled states as values of Δ_t from $t=1$ to $t=12$ are all zero. Observing such a phenomenon in VQE circuits requires depth around 48. Each point is obtained by averaging 4000 samples.

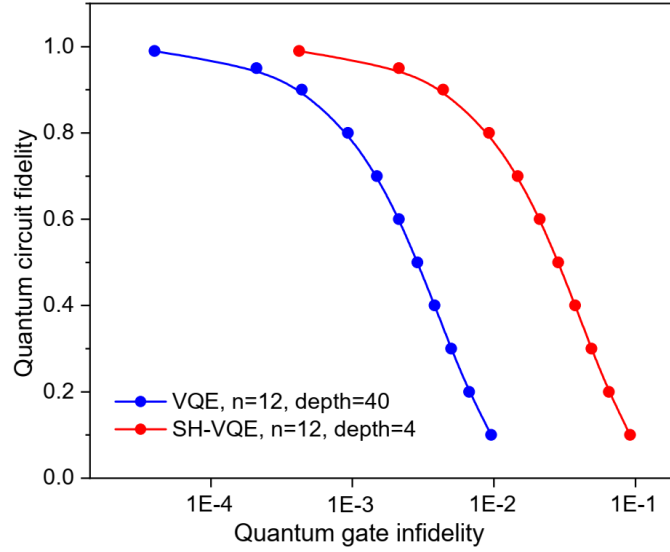


Figure S2: Fidelity requirement relief. The infidelities of 2-qubit blocks are plotted as functions of total circuit fidelity. The expressivity of 12-qubit 4-depth SH-VQE circuit is close to 12-qubit 40-depth VQE circuit whereas there is a huge difference of the fidelity requirement of gate blocks.

We further run numerical experiments to see the scalability of our algorithm. We treat expressivity as a measure of the equivalence of VQE circuit and SH-VQE circuit. The results of our algorithm are shown in Fig.S3, where we fix the SH-VQE Schrödinger circuit depth at 2 and 4 and show the equivalent VQE circuit depth as functions of the system size. From the figure, we can see that the more of the qubit number is, the more equivalent VQE circuit depth is achieved, which gives SH-VQE a growing advantage as the quantum device become larger and larger.

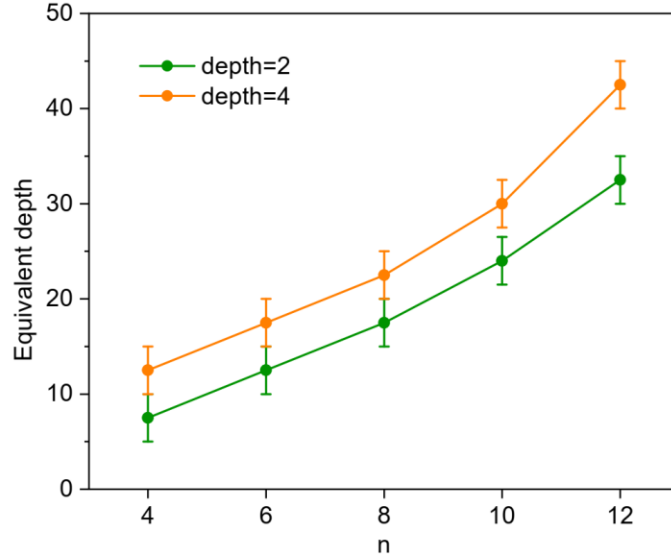


Figure S2: Algorithm scalability. For SH-VQE circuit, we fix the Schrödinger circuit depth at 2 and 4 and add Clifford circuits as the Heisenberg part. For different system sizes, we show the equivalent VQE circuit depth by comparing the expressivity. The depth improvement become stronger and stronger as the number of qubits increase.

3. The structure of parametrized circuit

The structure of parametrized circuits used when solving XXZ models is shown in Fig.S4.

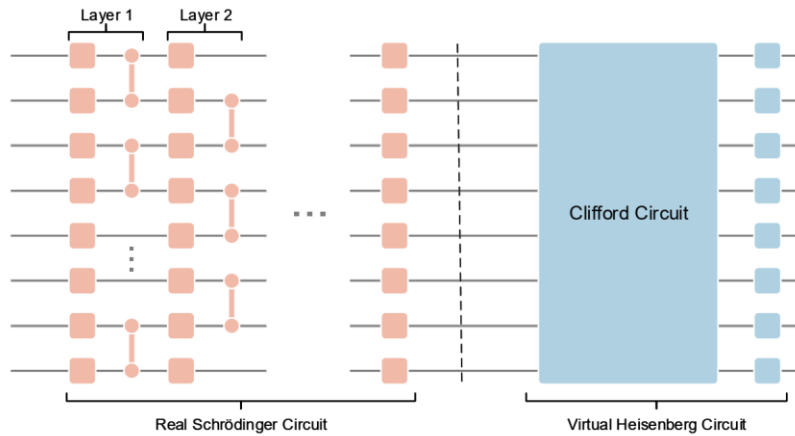


Figure S4: Structure of parametrized circuits used when solving XXZ models. Two-qubit gates are fixed CZ gates while each single-qubit gate is parametrized as $\exp(-i\theta_x\sigma_x)\exp(-i\theta_y\sigma_y)\exp(-i\theta_z\sigma_z)$. The Clifford part is composed of only CZ gates.

4. The expressibility and the trainability of SH-VQA

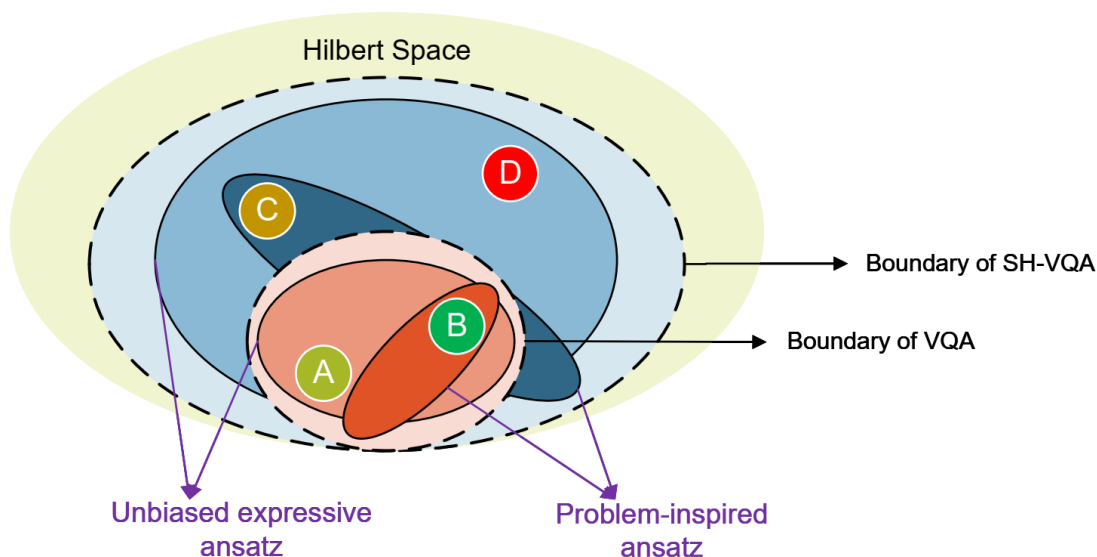


Figure S5: The expressibility and the trainability of SH-VQA. The motivation of our SH-VQA proposal is to go beyond VQA boundary set by the NISQ devices and give us more freedom to build the ansatzes. Given specific problems (A, B, C, D), we want to use the real quantum circuit to solve them. We can see that for VQA, we can only possibly solve problems A and B, since C and D are outside the VQA boundary. In the contrary, we are possible to solve all A, B, C, D by SH-VQA, which shows the advantages of our proposal. When really running the algorithms, we are required to build ansatzes. We know that for VQA, there are either unbiased ansatz with high expressibility but low trainability (e.g., the hardware-efficient ansatz) or problem-inspired ansatz with biased low expressibility and high trainability (e.g., the UCC and the HVA). Then, similar to the VQA, for SH-VQA, we can also expect to propose unbiased expressive ansatz or problem inspired ansatz.